Salt Gradient Modulation of MicroRNA Translocation through a Biological Nanopore

Josip Ivica,[†] Philip T. F. Williamson,[‡,§] and Maurits R. R. de Planque[†,§]

[†]Electronics and Computer Science, [‡]Centre for Biological Sciences, and [§]Institute for Life Sciences, University of Southampton, Southampton SO17 1BJ, United Kingdom

ABSTRACT: In resistive pulse sensing of microRNA biomarkers, selectivity is achieved with polynucleotide-extended DNA probes, with the unzipping of a miRNA−DNA duplex in the nanopore recorded as a resistive current pulse. As the assay sensitivity is determined by the pulse frequency, we investigated the effect of *cis*/*trans* electrolyte concentration gradients applied over α-hemolysin nanopores. KCl gradients were found to exponentially increase the pulse frequency, while reducing the preference for 3'-first pore entry of the duplex and accelerating duplex unzipping, all manifestations of an enhanced electrophoretic force. Unlike silicon nitride pores, a counteracting contribution from electro-osmotic flow along the pore wall was not apparent. Significantly, a gradient of 0.5 / 4 M KCl increased the pulse frequency ~60-fold with respect to symmetrical 1 M KCl, while the duplex dwell time in the nanopore remained acceptable for pulse detection and could be extended by LiCl addition. Steeper gradients caused lipid bilayer destabilization and pore instability, limiting the total number of recorded pulses. The 8-fold KCl gradient enabled a linear relationship between pulse frequency and miRNA concentration for the range 0.1−100 nM. This work highlights differences between biological and solid-state nanopore resistive pulse sensing and informs strategies for sub-nanomolar miRNA quantification with bilayer-embedded porins.

MicroRNA molecules (miRNAs), short non-coding RNAs that regulate post-transcriptional gene expression, are promising targets for novel therapeutic and diagnostic approaches.[1-3] Existing amplification-based miRNA quantification strategies suffer from drawbacks related to the very small, ~18-22 nt, RNA size, and typically give relative rather than absolute miRNA concentrations.[4-6] Instead, Wanunu *et al*. and Wang *et al*. established that specific miRNAs in a total RNA extract can be quantified by simply counting the number of molecules that traverse a nanopore.[7,8] Each translocation event is manifested as a transient current decrease because pore-confined miRNA displaces electrolyte ions.[9,10] This application of nanopore resistive pulse sensing requires an oligonucleotide probe selective for the miRNA species of interest, with assay sensitivity determined by the rate at which the miRNA−probe duplex is captured by the pore.[9,11-13] In contrast to nanopore sequencing where the main challenge is to obtain a low translocation speed of single-strand DNA/RNA,[14] quantification applications require optimization of the duplex capture rate.

When, driven by an applied potential, a miRNA-probe duplex enters a ~3 nm diameter solid-state pore, it traverses the pore at a similar speed as a single-strand oligonucleotide but gives a deeper current block.[7,12,14] For the biological nanopore α-hemolysin (αHL), a duplex blocks the pore entrance because the channel constriction is ~1.4 nm, whereas a non-hybridized oligonucleotide rapidly (~0.1 ms) translocates the pore.[8,12,15] After ~100−1000 ms the duplex dissociates in the αHL vestibule, with subsequent rapid pore translocation of the DNA and miRNA.[8,16] In order to accurately relate the stochastic current block events with analyte concentrations, ~200 translocation events need to be analyzed[7,17] in a time frame, imposed by assay throughput and pore stability considerations, of ~30 mins, implying a minimum event frequency of ~5 translocations per minute (~0.1 events s^{-1}). For a silicon nitride nanopore,

Wanunu *et al*. reported a linear relationship between duplex resistive pulse frequency and miRNA concentration from 100 nM (~100 events s^{-1}) down to 0.1 nM (~0.6 events s^{-1}), at a potential of 500 mV and with the conventional nanopore electrolyte solution of 1 M KCl.[7] For αHL, also with 1 M KCl, Wang *et al*. found a linear correlation from 100 nM (~0.2 events s^{-1}) down to 10 nM (~0.03 events s^{-1}) duplex at 100 mV.[8] Higher potentials lead to a higher duplex capture rate because of the stronger electrophoretic force, but for biological porins the potential is limited to ~150 mV due to the fragility of the lipid bilayer matrix.[18]

An alternative approach is to change the electrolyte solution. Studies in which [KCl] was varied equally on both sides of the pore focused exclusively on the translocation speed or did not show a substantial rate enhancement above ~0.5 M KCl.[19-21] However, Wanunu *et al*. demonstrated that the capture rate of 400-8000bp dsDNA for a silicon nitride nanopore is significantly enhanced by asymmetrical KCl solutions, with a linear relationship between gradient asymmetry and rate enhancement when $[KCl]_{trans}/[KCl]_{cis} > 1.5$. For example with a 20-fold *cis*/*trans* gradient of 0.2 / 4 M KCl, the dsDNA capture rate increased 30-fold.[22] Interestingly, under the same conditions the dwell time increased 3-fold to ~20 ms, implying a reduced dsDNA translocation speed. The authors postulated that salt gradients enhance the electric funneling field near the pore entrance, and also increase the electro-osmotic counterflow inside the pore,[22] which was later supported by a number of comprehensive theoretical studies on KCl salt gradients over solid-state nanopores.[23-32] Kowalczyk *et al*. also investigated alternative electrolyte species, concluding that DNA dwell times in a silicon nitride pore increase when symmetrical KCl is replaced with NaCl or LiCl because of stronger DNA binding of these smaller cations.[33]

For αHL, there is very limited data on DNA capture rate enhancement by alternative electrolyte solutions. Results from experimental and theoretical solid-state pore studies cannot readily be extrapolated because of the smaller porin dimensions, necessitating duplex unzipping, and the non-uniform shape and charge distribution of porin channels, which affect ion distribution and therefore capture and translocation forces.[34,35] It was recently reported that replacing KCl with symmetrical 1 M tetramethylammonium chloride (TMA-Cl) enhances the capture rate of poly(dC)$_{25}$ ~3-fold at 120 mV while the dwell time increases slightly, with more pronounced effects at higher symmetrical TMA-Cl concentrations.[36] Johnson *et al*. investigated dsDNA duplex unzipping times in the αHL pore for seven different monovalent chloride salts, all at symmetrical 1 M concentration, and observed substantially longer dwell times for NaCl, and LiCl than for KCl. Strong DNA association of these cations may present an energetic barrier at the αHL constriction site.[37]

Jeon and Muthukumar recently studied the effect of KCl gradients on poly(styrenesulfonate) capture by αHL over a wide range of salt gradients and applied potential.[38,39] For example with a 10-fold *cis/trans* gradient of 0.2 / 2 M KCl, the capture rate increased ~20-fold with respect to symmetrical 1 M KCl at 140 mV.[38] In a second study with smaller gradients they observed a *decreased* translocation time, e.g. 1.6 ms for symmetrical 1 M KCl and 1.0 ms for 0.5 / 1 M KCl at 140 mV.[39] Gu and co-workers authored a large body of work about miRNA detection with αHL at symmetrical 1 M KCl, addressing the duplex-pore interaction mechanism and also implementing original modifications, e.g. multiplexing and anti-field capture.[16,17,40,41] To support a clinical RNA extract study, they employed a 0.2 / 3 M KCl gradient, obtaining a linear relationship between miRNA–DNA duplex event frequency and miRNA concentration from 0.1 pM (~0.01 events s^{-1}) to 100 pM (~0.04 events s^{-1}), extending the

10 – 100 nM range measured with symmetrical 1 M KCl.[8] However, to date, the effects of salt gradients on miRNA sensing with a biological porin remain to be explored systematically.

In this paper, we investigate miRNA–DNA duplex interactions with αHL for a range of *cis*/*trans* KCl gradients. We also verify DNA probe design under asymmetric electrolyte conditions and evaluate electrolytes other than KCl. The electrolyte gradients are found to exponentially enhance DNA duplex capture by αHL but to considerably decrease the miRNA dwell time, a marked difference with silicon nitride pores. This is consistent with a gradient-enhanced electrophoretic force and a weak counteracting EOF. Addition of LiCl results in slower duplex unzipping. Excessive gradients or potentials destabilize the bilayer, hence an 8-fold KCl gradient at 120 mV is selected to establish the relation between duplex concentration and capture rate, yielding insight in the opportunities and limitations of miRNA quantification with αHL resistive pulse sensing.

MATERIALS AND METHODS

The target sequences miR155, miD155 and the $(dC)_{30}$-extended DNA probes (Table S1) were obtained from Sigma Aldrich. Probe-target hybridization conditions are described in the SI. Wild-type *S. aureus* α-hemolysin (αHL) (Sigma Aldrich) was dissolved in deionized water to 0.1 mg/mL. The phospholipid 1,2-diphytanoyl-*sn*-glycero-3-phosphocholine (Avanti Polar Lipids) was dissolved in chloroform to 20 mg/mL. The two Delrin chambers of a bilayer recording setup were filled with 1 mL of buffered (10 mM Tris (pH 8.0), 1 mM EDTA) electrolyte solution (e.g. 1 M KCl). Lipid bilayers were suspended in apertures in a polytetrafluoroethylene sheet by the

monolayer folding method.[42] Following *cis* side addition of 1 μL of αHL solution the bilayer current was monitored until a single αHL pore formed in the bilayer. DNA duplex was then added to the *cis* compartment and pore translocations towards the *trans* side (active Ag/AgCl electrode) were subsequently induced by applying a positive potential. Bilayer currents were measured with an Axopatch 200B (Molecular Devices) current amplifier, sampled at 50 kHz with a DigiData 1440 digitizer (Molecular Devices) and filtered with a 10 kHz built-in Bessel filter. Resistive pulses shorter than 1 ms were excluded from the current trace analysis. Event dwell times (τ_{off}) and interevent intervals (τ_{on}) were analyzed in Clampfit 10.2 (Molecular Devices) as log-binned histograms (see SI). Standard deviations were derived from independent experiments (e.g. Table S3).

RESULTS AND DISCUSSION

We selected the miRNA target miR155, implicated in lung cancer, and its complementary DNA probe P155, with 5' and 3' terminal poly$(dC)_{30}$ extensions (Table S1), previously studied by nanopore resistive pulse sensing.[8,16] Lipid bilayers formed in laser-cut apertures exhibited excellent mechanical stability and long lifetimes, up to a day, in buffered symmetrical 1 M KCl electrolyte at a potential of ≤120 mV. Following insertion of a single α-hemolysin (αHL) pore, an open-pore current could be observed for ~1 hour, occasionally interrupted by closed-pore episodes.[43] For practical reasons most experiments were performed with miD155, the DNA equivalent of miR155.[16] With the miD155–P155 DNA duplex, *i.e.* miD155 hybridized to P155, added to the *cis* compartment, transient αHL current block events, corresponding to duplex capture by the αHL pore, were observed (Figure 1a). The blocked-pore current sometimes

persisted for a prolonged period of time (>20 s) and only reverted to the open-pore current after briefly switching the voltage polarity. This has been attributed to pore clogging by nucleotide fragments, potentially folded into a 3D structure.[41,43]

Selecting a concentration of 100 nM miD155–P155 duplex and symmetrical *cis*/*trans* 1 M KCl electrolyte as our reference conditions, we first analyzed the amplitude and the duration of the resistive pulses obtained at +120 mV. A representative current trace with several current-block events is shown in Figure 1a. An expanded view of a single event is shown in Figure S1. Level 0 is the open-pore current I_0 of ~115 pA, level 1 is the residual current (~10% of I_0) when the vestibule of the αHL pore is occupied by a DNA duplex.[8,16] The level 1 dwell times spanned a wide range and could last up to ~10 s (Figure 1b). The mean event dwell time (τ_{off}) and interevent interval (τ_{on}) were determined by fitting log-binned histograms (e.g. Figure 1b-c) with an exponential probability function (Table S2). The event time was found to be 1.043 ± 0.013 s while the interevent interval was 5.167 ± 1.264 s (Table S3). This is in agreement with previous work on αHL resistive pulse sensing of miR155–P155 in 1 M KCl,[8] except that we observed two distinct values of the level 1 current, 0.098 and 0.13 I/I_0 (Figure 1d and 1e) instead of a single amplitude of 0.15 I/I_0.[8] As discussed below, we relate this to the directionality of P155 pore entry.

The capture of analyte molecules by the pore is the rate limiting step in oligonucleotide-nanopore interactions.[8,16,22,44] This can be quantified as $f_{on} = k_{on}$ [duplex], with $f_{on} = 1/\tau_{on}$ (events s^{-1}) representing the capture rate, also referred to as the event frequency, [duplex] the concentration of the miRNA–probe duplex and k_{on} (events s^{-1} M^{-1}) the occurrence rate constant of duplex capture events.[8] The event frequency, in combination with recording time limitations, determines the sensitivity and the limit of quantification of the nanopore assay. For 100 nM

miD155–P155 in symmetrical 1 M KCl at +120 mV, the frequency is 0.2 ± 0.04 s^{-1}, *i.e.* it takes ~10 mins to obtain 100 resistive pulses. A similar frequency was obtained with miR155–P155 duplexes (Figure S9). Increasing the applied potential and thereby the electrophoretic force results in a higher oligonucleotide capture rate,[7,22] linearly increasing over the range 100 – 180 mV.[16] We obtained k_{on} values of 9.2 ± 1.8 μM^{-1} s^{-1} at 150 mV and 17.6 ± 0.4 μM^{-1} s^{-1} at 180 mV, with respective dwell times τ_{off} of 10.67 ± 1 and 2.4 ± 0.1 ms. This represents a linear increase of k_{on} (Figure 1f) but a non-linear decrease of τ_{off} (Figure 1g), also observed by Perera *et al.* for short DNA duplexes.[45] Although the capture rate was 8-fold increased at 180 mV, the duplex unzipping step was thus accelerated ~450-fold. Given that a τ_{off} value of 2.4 ms is close to the typical duplex capture criterion of τ_{off} > 1 ms, a potential exceeding 180 mV will render event detection problematic. Also considering that the bilayer lifetime is reduced at potentials >120 mV, an alternative strategy for improving the sensitivity of the nanopore assay is required.

Effects of *cis*/*trans* KCl gradient on duplex capture and translocation. We systematically investigated the effect of a range of KCl gradients on the αHL nanopore translocation properties of miD155–P155 duplexes. Figure 2a shows that with 4 M KCl rather than 1 M KCl in the *trans* chamber, the duplex-αHL current block events occurred at 10-fold higher frequency (interevent interval τ_{on} reduced from 5.180 ± 1.248 s to 0.190 ± 0.028 s) while the τ_{off} decreased 16-fold, from 1042 ± 13 to 66.8 ± 3.4 ms. These effects were reversible; gradually replacing the *trans* solution to obtain 1 M KCl, without disturbing the αHL pore, restored the k_{on}, τ_{on} and τ_{off} parameters typical for symmetrical 1 M KCl conditions.

Why does a *cis*/*trans* salt gradient result in a higher duplex capture rate and a shorter duplex dwell time in the αHL pore? KCl gradients are thought to contribute to the localized

electric funneling field at the *cis* side of the pore, rather than to the global field experienced by the entire lipid bilayer, because cations have to accumulate there to meet the requirement for a continuous current flow along the pore axis.[22,24,27,28] Oligonucleotides therefore experience a larger electrophoretic force near the pore entrance than with symmetrical KCl, and faster duplex unzipping, observed in our experiments as a shorter level-1 state, is thus expected in the absence of substantial counteracting forces. Silicon nitride pores have a high surface charge density (~ -35 mC/m^2 at pH 8.5),[46] hence the gradient-enhanced *trans*-to-*cis* EOF can be sufficiently strong to reduce the translocation speed, i.e. *increase* the dwell time.[22,28,30,47,48] Moreover, EOF is more sensitive to a salt gradient than the electrophoretic force.[24] For the αHL pore with its heterogeneous charge distribution, EOF is known to be significantly weaker,[49,50] which explains the observed *decrease* in dwell time of poly(styrenesulfonate)[39,51] and of DNA duplexes when a salt gradient is applied.

Given that 4 M KCl is close to the solubility limit, the effect of a *cis*/*trans* KCl gradient was investigated by maintaining 4 M KCl in the *trans* chamber and varying $[KCl]_{cis}$ from 2 to 0.1 M, *i.e*. from a 2-fold to a 40-fold gradient. Representative current traces for 8-fold and 40-fold gradients, shown in Figure 2a, illustrate the further decrease in τ_{off} and in τ_{on} with respect to the 4-fold gradient of 1 M / 4 M KCl. The event frequency increased exponentially from 0.81 ± 0.1 s^{-1} (2 M / 4 M KCl) to 38.2 ± 8.1 s^{-1} (0.1 M / 4 M KCl), a more substantial increase then observed by Wanunu *et al*.,[22] while the event dwell time decreased from 415 ± 10 ms to 5.44 ± 0.5 ms (Figure 2b). For 100 nM duplex at an applied potential of 120 mV, the 40-fold KCl gradient thus resulted in an impressive ~200-fold increase in capture rate, but a ~170-fold decrease in αHL block duration, compared to 1 M symmetrical KCl. This *gradient*-induced exponential translocation rate enhancement, also observed with $[KCl]_{trans}$ <4 M (Figure S5), is

similar to the *potential*-induced rate enhancement previously observed with αHL for miRNA155–P155 duplex[8] or 92-nt ssDNA[44] in symmetrical 1 M KCl, supporting the notion that the gradient leads to a stronger electric funneling field at the *cis* nanopore entrance.[22,24]

Unfortunately, the 20- and 40-fold gradients destabilized the lipid bilayer, most likely because of excessive osmotic pressure,[52,53] and the αHL pores regularly closed, possibly because of an increased bilayer line tension[54] or a relatively low KCl concentration[55] in the *cis* compartment. Also with the 0.5 / 4 M KCl gradient, bilayer and pore stability were reduced with respect to symmetrical 1 M KCl conditions (Figure S6), but because it was typically possible to monitor current resistive pulses for ~20 mins with the same nanopore, we selected this 8-fold gradient for further characterization of nanopore translocation. For 100 nM miD155–P155 duplex and at 120 mV (Table S5), the event frequency was 12.5 ± 1 s^{-1} and the dwell time 33.5 ± 9.0 ms, with similar values for miR155–P155 duplex (Figure S10), but these values strongly depend on the applied potential. As shown in Figure 2c, the event frequency at 100 mV was only 1.03 ± 0.22 s^{-1}, increasing exponentially to 65.7 ± 4.6 s^{-1} at 180 mV. With respect to symmetric 1 M KCl electrolyte (Figure 1f), the 0.5 / 4 M KCl system enabled a 62-, 43- and 40-fold increase in the event frequency at 120, 150 and 180 mV, respectively. The relation between the event dwell time and the applied voltage was also exponential for the 8-fold gradient (Figure 2c, right panel), decreasing from 700 ms at 100 mV to just 2 ms at 180 mV. This is a larger reduction in dwell time than seen in Figure 1g and is also more pronounced than previously reported for 100 nM miR155 duplex[16] and for 23-nt dsDNA[45] in symmetrical 1 M KCl, again illustrating the contribution of the gradient to the electrophoretic force.

Modulation of duplex dwell time by electrolyte species. To gain further insight in electrolyte modulation of duplex-αHL interactions with electrolytes other than KCl,[33,36,37] we first performed experiments with 100 nM miD155−P155 in symmetrical 1 M KCl, NaCl, CsCl, NH_4Cl and LiCl solutions at 120 mV. As shown in Table 1, we found similar dwell times of ~1 s for all these electrolytes with the exception of LiCl, which resulted in such long-lived level-1 current block events, over 20 s in duration, that determination of the event frequency was not pursued. At 180 mV, dwell times were reduced to ~2 − 5 ms, while LiCl resulted in a dwell time of 41 ms (Table S7). For the other cations, the event frequency increased in the order $NH_4^+ > Cs^+ \approx Na^+ > K^+$ but, at 120 mV, also in NH_4Cl the frequency did not exceed ~0.5 s^{-1}.

We then performed experiments with various electrolyte gradients at 120 mV, focusing on CsCl because this is more soluble (up to 11 M at 20 °C) than KCl and on LiCl because this results in longer dwell times. A *cis/trans* gradient of 0.5 / 4 M CsCl gave a similar enhancement of the event frequency as 0.5 / 4 M KCl, but a longer dwell time of ~45 s (Table 1). The effect of gradients with a $[CsCl]_{trans}$ >4 M could not be analyzed because of bilayer destabilization. The use of a 0.5 / 4 M LiCl gradient resulted in an excessively long dwell time, exceeding 5 s, rendering event collection impractical. At 150 mV, however, this LiCl gradient resulted in a dwell time of 102 ± 48 ms, ~30 times longer than for the equivalent KCl gradient at this potential, but a 4-fold reduced frequency of ~8 s^{-1}. Duplex translocation characteristics for various gradients at 150 mV and 180 mV are presented in Table S8. Interestingly, a mixed-electrolyte gradient of 0.5 M LiCl (*cis*) and 4 M KCl (*trans*) resulted in a similar capture rate as with the 0.5 / 4 M KCl gradient, while the dwell time was increased approximately 2-fold, to 63 ± 7.5 ms. Although the exact concentrations of KCl and LiCl in close proximity to the nanopore are likely to depend on electrolyte diffusion through the nanopore, it is apparent that a KCl

gradient-induced reduction in the dwell time can, to some extent, be compensated by the addition of LiCl.

Influence of DNA probe design under KCl gradient conditions. DNA probes for miRNA nanopore resistive pulse sensing consist of a central sequence, complementary to the target miRNA, with flanking 3' and 5' overhang sequences which, up to a length of 30 nucleotides,[16] facilitate pore capture. Counterintuitively, for symmetrical 1 M KCl and at 100 mV, Wang *et al*. observed that the capture rate of a P155 DNA probe with only a 3' terminal poly(dC)$_{30}$ overhang is 20 times higher than that of a 5'-overhang probe.[8] To understand the role of the probe extensions on duplex-pore interactions in the presence of a KCl gradient, we used the single-overhang DNA probes P155-3'-(dC)$_{30}$ and P155-5'-(dC)$_{30}$, which only have a (dC)$_{30}$ extension at the 3' or the 5' terminus. As shown in Figure 3b-c and in Table 2, duplexes with miD155 hybridized to P155-3'-(dC)$_{30}$ gave a single block level of I/I_0 = 0.096, while duplexes with P155-5'-(dC)$_{30}$ gave a single block level of I/I_0 = 0.128 (Table 2).

For the bimodal I/I_0 distribution obtained with the double-overhang probe (Figure 3a), we could thus assign the population centered at 0.096 I/I_0 (55% of all events) to duplex pore entry by the 3' probe terminus and the population at 0.131 I/I_0 (45% of all events) to 5'-first entry (Table S6). With a 0.5 / 4 M KCl gradient, the pore capture rate was hence similar for 3'-first and 5'-first pore entry of the double-overhang P155 probe. This was not the case under symmetrical 1 M KCl conditions (Figure 1 d-e), where the deep-block events at 0.10 I/I_0 (assigned to 3'-first pore entry) were nearly three times more abundant than the 5'-first entry events at 0.13 I/I_0 (Table S4). In symmetrical 1 M KCl, Meller *et al*. also observed two distinct αHL block levels for single-strand (dA)$_{100}$ and (dC)$_{100}$, with ~3-fold more events at the deeper block level.[15] These

observations suggest that, in the absence of a salt gradient, pore entry with the 3' terminus is energetically more favorable than 5'-first entry.

As the cytosine bases are slightly tilted, with respect to the phosphate backbone, towards the 5' terminus, the pore confinement-induced change in tilt angle is in the preferred 5' direction when pore capture and translocation occurs 3'-first.[56-59] In contrast, 5' entry will necessitate base reorientation with concomitant friction effects, an energy cost that is manifested as a lower probability of pore entry.[56-59] It appears that for the 0.5 / 4 M KCl gradient (Figure 3a), unlike for the symmetrical 1 M KCl system (Figure 1e), miRNA-probe duplexes experience a sufficiently large, gradient-enhanced, electrophoretic force that such subtle orientation-dependent nucleotide-pore interactions cannot significantly influence the capture rate.

This implies that for symmetrical 1 M KCl but at an applied potential >120 mV, the event frequency of 3'-first and 5'-first pore capture should also be similar, which was indeed observed for miD155−P155 duplexes at 180 mV (data not shown). However, the residual nanopore current remains sensitive to the conformation of pore-confined molecules; the shallower current block of 5'-first entry duplexes occurs under both symmetric and asymmetric electrolyte conditions (Figure 1d-e & 3a) because ions can pass a captured oligonucleotide with reoriented bases more readily.[56,57] Moreover, for duplexes with the full-length P155 probe, the dwell time of 3'-first entry duplexes is approximately twice as long as for 5'-entry duplexes, for both 0.5 / 4 M KCl (Table 2) and symmetrical 1 M KCl (Table S4).

The single-overhang DNA probes also illustrate another aspect of DNA-pore interactions: long-lived (seconds) level 1 currents that rapidly (ms) fluctuate between ~20 pA (0.11 I/I_0) and ~50 pA (0.28 I/I_0), resembling a gating ion channel (Figure S11). With symmetric 1 M KCl electrolyte at 120 mV, this particular current signature was previously observed with blunt-end

DNA duplexes lacking any overhang sequence, and was attributed to transient threading of a partially unzipped duplex into the αHL constriction channel.[45,60] Although of shorter duration, we also observed these episodes with the 0.5 / 4 M KCl gradient at 150 and 180 mV (data not shown), indicating that also with an increased electrophoretic force, single-overhang duplexes that enter the αHL vestibule by their blunt end are not readily unzipped. A double-overhang sequence is thus an essential element of a DNA probe for miRNA resistive pulse sensing.

Number of translocation events for lower duplex concentrations. With the 0.5 / 4 M KCl gradient and an applied potential of 120 mV, conditions that maximize the event frequency while avoiding excessive bilayer destabilization or αHL pore closures, we evaluated the frequency of miD155–P155 duplex capture events for a range of duplex concentrations, from our reference concentration of 100 nM down to 10 pM. Because duplex capture by the nanopore is a stochastic event, the interevent intervals are exponentially distributed (e.g. Figure 1c, Figure S2) and obtaining mean values by histogram fitting requires, in our experience, approximately 200 events. As shown in Figure 4a, the recording of resistive pulses is interrupted by pore closures, which occur less frequently at lower duplex concentration. Figure 4b shows distributions of open-pore durations, with mean values of 5.4 s ms for 100 nM duplex (primarily nucleotide-clogged pores) and 27 s for 1 nM duplex (primarily spontaneous pore closures). The pore can typically be re-opened by briefly reversing the potential (see above) and resistive pulses from subsequent open-pore episodes can be pooled for determination of the mean interevent intervals.

We observed a linear relation between the duplex concentration and the event frequency (Figure 4c), in agreement with previous miRNA studies with solid-state and αHL pores,[7,8] over the range 100 nM – 100 pM. The error in the mean event frequency was calculated from

independent experiments. It should be noted that below a duplex concentration of 10 nM, a single experiment does not yield sufficient resistive pulses for histogram analysis, hence the event frequency was obtained by dividing the number of pulses by the total open-pore time (see also Figure S12). For 1 nM, 500 pM and 100 pM duplex, on average 72, 20 and 10 resistive pulses were acquired within a single experiment, but at 10 pM concentration not a single pulse was observed during several minutes of recording. The mean event frequency at 100 pM duplex was determined as 0.027 ± 0.011 s^{-1}. The error is substantial because of the large difference between individual experiments, in itself due to the very small number of events (0–2 per open-pore episode).

Wang *et al*. determined the αHL translocation frequency of miR155-P155 with a 15-fold (0.2 / 3 M) KCl gradient for the range 0.1 – 100 pM, at 120 mV.[8] They reported an event frequency of ~0.04 s^{-1} for 100 pM duplex, similar to the value obtained with our 8-fold gradient, and a frequency of ~0.01 s^{-1} for 0.1 pM duplex.[8] However, for duplex concentrations <100 pM we were unable to collect a sufficient number of events in individual experiments in a practical timeframe. Wanunu *et al*. measured the event frequency of a 25-bp dsDNA sequence down to 100 pM concentration, reporting a relatively high frequency of ~0.5 s^{-1} in symmetrical 1 M KCl, but their solid-state nanopore enabled them to apply a potential of 500 mV.[7] This is not possible with bilayer-incorporated biological nanopores. Indeed, in our system the frequency-enhancing effect of increasing the voltage to 150 or 180 mV was offset by the concomitant reduction in bilayer lifetime (data not shown).

Under our experimental conditions, where an aperture-suspended lipid bilayer is positioned in between two compartments of 1 mL volume, we consider 100 pM duplex as the limit of miRNA quantification. The concentrations of individual miRNA species in human plasma is

approximately in the range 0.1 – 1 pM,[61,62] but because samples for nanopore analysis are processed as total miRNA extracts[7,8] it is the extract resuspension step that determines the miRNA concentration of the probed sample. In the critically important RNA extraction protocol,[63] the silica-immobilized RNA should thus be resuspended in a minimal volume. For example, with 1 mL of plasma containing ~0.1 – 1 fmol of individual miRNA species, extract resuspension in a 1 μL volume would give a concentration range of ~0.1 – 1 nM. Volumes as small as ~1 μL are suitable for miniaturized bilayer electrophysiology and hence for nanopore resistive pulse sensing with droplet-in-oil systems, which can also be implemented as arrays for high-throughput assays.[64-67] Alternatively, a sample could be probed with multiple electrically independent nanopores, an approach that is similar to the development of high-throughput nanopore DNA sequencing.[68,69]

CONCLUSIONS

In summary, steeper salt gradients resulted in an exponential increase in the capture rate of probe-conjugated miRNA by αHL, indicative of a larger effective electrophoretic force near the pore entrance. The event dwell time decreased, typical for a weak EOF in a biological porin. However, this undesirable effect could be mitigated by a mixed-electrolyte gradient of LiCl and KCl. Also under gradient conditions, the double-$(dC)_{30}$ probe design is essential for duplex unzipping in the nanopore. Probes with a single overhang confirmed that the current block depth of translocation events depends on the direction of nanopore entry, highlighting the exquisite sensitivity of nanopore sensing. Unfortunately, just as with applying a higher potential, steeper gradients came at the cost of decreased bilayer stability. Pore closures were also more prominent

than in symmetrical 1 M KCl, although this may not occur with other porins. Bilayer and pore stability with salt gradients warrant further investigation. The 8-fold gradient offered a compromise between an enhanced capture rate and a reduced effective recording time, enabling determination of event frequencies down to 100 pM duplex. For quantification rather than detection, the stochastic nature of duplex capture necessitates analysis of ~200 events in independent experiments.[7,17] With 1 mL recording chambers, this was achieved for miRNA-probe concentrations ≥10 nM. Resuspending RNA extracts in smaller volumes for miniaturized sample compartments is expected to enable quantification of (patho)physiological miRNA levels by nanopore sensing with biological porins.

ASSOCIATED CONTENT

Supporting Information

The Supporting Information is available free of charge on the ACS Publication website at DOI:

Detailed experimental procedures, oligonucleotide sequences, resistive pulse signature, determination of resistive pulse parameters, 3' and 5' entry assignment of P155−miD155 events, additional KCl gradient analysis, traces with pore block episodes, voltage dependence of resistive pulse parameters for various electrolyte species, blunt-end duplex threading, and microRNA control experiments (PDF)

AUTHOR INFORMATION

Corresponding Author

*E-mail: mdp@ecs.soton.ac.uk

Notes

The authors declare no competing financial interests.

ACKNOWLEDGMENTS

J.I. was awarded a studentship from the University of Southampton. We thank Shengmiao Zhou for assistance with miRNA control experiments.

REFERENCES

(1) Wang, J.; Chen, J.; Sen, S. *J. Cell. Physiol.* **2016**, *231*, 25–30.

(2) Planell-Saguer, M.; Rodicio, M. C. *Clin. Biochem.* **2013**, *46*, 869–878.

(3) Graybill, R. M.; Bailey, R. C. *Anal. Chem.* **2016**, *88*, 431–450.

(4) Murphy, J.; Bustin, S. A. *Expert Rev. Mol. Diagn.* **2009**, *9*, 187–197.

(5) Schwarzenbach, H.; da Silva, A. M.; Calin, G.; Pantel, K. *Clin. Chem.* **2015**, *61*, 1333–1342.

(6) Marzi, M. J.; Montani, F.; Carletti, R. M.; Dezi, F.; Dama, E.; Bonizzi, G.; Sandri, M. T.; Rampinelli, C.; Bellomi, M.; Maisonneuve, P.; Spaggiari, L.; Veronesi, G.; Bianchi, F.; Di Fiore, P. P.; Nicassio, F. *Clin. Chem.* **2016**, *62*, 743–754.

(7) Wanunu, M.; Dadosh, T.; Ray, V.; Jin, J.; McReynolds, L.; Drndic, M. *Nat. Nanotechnol.* **2010**, *5*, 807–814.

(8) Wang, Y.; Zheng, D.; Tan, Q.; Wang, M. X.; Gu, L. Q. *Nat. Nanotechnol.* **2011**, *6*, 668–674.

(9) Reiner, J. E.; Balijepalli, A.; Robertson, J. W.; Campbell, J.; Suehle, J.; Kasianowicz, J. J. *Chem. Rev.* **2012**, *112*, 6431–6451.

(10) Miles, B. N.; Ivanov, A. P.; Wilson, K. A.; Dogan, F.; Japrung, D.; Edel, J. B. *Chem. Soc. Rev.* **2013**, *42*, 15–28.

(11) Kong, J.; Bell, N. A.; Keyser, U. F. *Nano Lett.* **2016**, *16*, 3557–3562.

(12) Gu, L. Q.; Wanunu, M.; Wang, M. X.; McReynolds, L.; Wang, Y. *Expert Rev. Mol. Diagn.* **2012**, *12*, 573–584.

(13) Kasianowicz, J. J.; Balijepalli, A. K.; Ettedgui, J.; Forstater, J. H.; Wang, H.; Zhang, H.; Robertson, J. W. *Biochim. Biophys. Acta* **2016**, *1858*, 593–606.

(14) Carson, S.; Wanunu, M. *Nanotechnology* **2015**, *26*, 074004.

(15) Meller, A.; Nivon, L.; Brandin, E.; Golovchenko, J.; Branton, D. *Proc. Natl. Acad. Sci. U. S. A.* **2000**, *97*, 1079–1084.

(16) Wang, Y.; Tian, K.; Hunter, L. L.; Ritzo, B.; Gu, L. Q. *Nanoscale* **2014**, *6*, 11372–11379.

(17) Zhang, X.; Wang, Y.; Fricke, B. L.; Gu, L. Q. *ACS Nano* **2014**, *8*, 3444–3450.

(18) Haque, F.; Li, J.; Wu, H. C.; Liang, X. J.; Guo, P. *Nano Today* **2013**, *8*, 56–74.

(19) Smeets, R. M.; Keyser, U. F.; Krapf, D.; Wu, M. Y.; Dekker, N. H.; Dekker, C. *Nano Lett.* **2006**, *6*, 89–95.

(20) Bonthuis, D. J.; Zhang, J.; Hornblower, B.; Mathé, J.; Shklovskii, B. I.; Meller, A. *Phys. Rev. Lett.* **2006**, *97*, 128104.

(21) Ghosal, S. *Phys. Rev. Lett.* **2007**, *98*, 238104.

(22) Wanunu, M.; Morrison, W.; Rabin, Y.; Grosberg, A. Y.; Meller, A. *Nat. Nanotechnol.* **2010**, *5*, 160–165.

(23) Hatlo, M. M.; Panja, D.; van Roij, R. *Phys. Rev. Lett.* **2011**, *107*, 068101.

(24) He, Y. H.; Tsutsui, M.; Scheicher, R. H.; Fan, C.; Taniguchi, M.; Kawai, T. *Biophys. J.* **2013**, *105*, 776–782.

(25) He, Y. H.; Tsutsui, M.; Scheicher, R. H.; Miao, X. S.; Taniguchi, M. *ACS Sensors* **2016**, *1*, 807–816.

(26) Liu, K. L.; Hsu, J. P.; Tseng, S. *Langmuir* **2013**, *29*, 9598–9603.

(27) Yeh, L. H.; Hughes, C.; Zeng, Z.; Qian, S. *Anal. Chem.* **2014**, *86*, 2681–2686.

(28) Lin, C. Y.; Yeh, L. H.; Hsu, J. P.; Tseng, S. *Small* **2015**, *11*, 4594–4602.

(29) Lin, J. Y.; Lin, C. Y.; Hsu, J. P.; Tseng, S. *Anal. Chem.* **2016**, *88*, 1176–1187.

(30) Hsu, W. L.; Daiguji, H. *Anal. Chem.* **2016**, *88*, 9251–9258.

(31) Zhai, S.; Zhao, H. *Phys. Rev. E* **2016**, *93*, 052409.

(32) Zhang, Y.; Wu, G.; Si, W.; Ma, J.; Yuan, Z.; Xie, X.; Liu, L.; Sha, J.; Li, D.; Chen, Y. *Nanoscale* **2017**, *9*, 930–939.

(33) Kowalczyk, S. W.; Wells, D. B.; Aksimentiev, A.; Dekker, C. *Nano Lett.* **2012**, *12*, 1038–1044.

(34) Aksimentiev, A. *Nanoscale* **2010**, *2*, 468–483.

(35) Firnkes, M.; Pedone, D.; Knezevic, J.; Doblinger, M.; Rant, U. *Nano Lett.* **2010**, *10*, 2162–2167.

(36) Wang, Y.; Yao, F.; Kang, X. F. *Anal. Chem.* **2015**, *87*, 9991–9997.

(37) Johnson, R. P.; Fleming, A. M.; Burrows, C. J.; White, H. S. *J. Phys. Chem. Lett.* **2014**, *5*, 3781–3786.

(38) Jeon, B. J.; Muthukumar, M. *J. Chem. Phys.* **2014**, *140*, 015101.

(39) Jeon, B. J.; Muthukumar, M. *Macromolecules* **2016**, *49*, 9132–9138.

(40) Tian, K.; Decker, K.; Aksimentiev, A.; Gu, L. Q. *ACS Nano* **2017**, *11*, 1204–1213.

(41) Gu, L. Q.; Wang, Y. *Methods Mol. Biol.* **2013**, *1024*, 255–268.

(42) Kalsi, S.; Powl, A. M.; Wallace, B. A.; Morgan, H.; de Planque, M. R. *Biophys. J.* **2014**, *106*, 1650–1659.

(43) Maglia, G.; Henricus, M.; Wyss, R.; Li, Q.; Cheley, S.; Bayley, H. *Nano Lett.* **2009**, *9*, 3831–3836.

(44) Maglia, G.; Restrepo, M. R.; Mikhailova, E.; Bayley, H. *Proc. Natl. Acad. Sci. U. S. A.* **2008**, *105*, 19720–19725.

(45) Perera, R. T.; Fleming, A. M.; Peterson, A. M.; Heemstra, J. M.; Burrows, C. J.; White, H. S. *Biophys. J.* **2016**, *110*, 306–314.

(46) Hoogerheide, D. P.; Garaj, S.; Golovchenko, J. A. *Phys. Rev. Lett.* **2009**, *102*, 256804.

(47) Lu, B.; Hoogerheide, D. P.; Zhao, Q.; Yu, D. *Phys. Rev. E Stat., Nonlinear, Soft Matter Phys.* **2012**, *86*, 011921.

(48) Katkar, H. H.; Muthukumar, M. *J. Chem. Phys.* **2014**, *140*, 135102.

(49) Piguet, F.; Discala, F.; Breton, M. F.; Pelta, J.; Bacri, L.; Oukhaled, A. *J. Phys. Chem. Lett.* **2014**, *5*, 4362–4367.

(50) Boukhet, M.; Piguet, F.; Ouldali, H.; Pastoriza-Gallego, M.; Pelta, J.; Oukhaled, A. *Nanoscale* **2016**, *8*, 18352–18359.

(51) Wong, C. T.; Muthukumar, M. *J. Chem. Phys.* **2010**, *133*, 045101.

(52) Ohki, S. *J. Membr. Biol.* **1984**, *77*, 265–275.

(53) Logisz, C. C.; Hovis, J. S. *Biochim. Biophys. Acta* **2005**, *1717*, 104–108.

(54) Kinnun, J. J.; Mallikarjunaiah, K. J.; Petrache, H. I.; Brown, M. F. *Biochim. Biophys. Acta* **2015**, *1848*, 246–259.

(55) Kasianowicz, J. J.; Bezrukov, S. M. *Nat. Biotechnol.* **2016**, *34*, 481–482.

(56) Purnell, R. F.; Mehta, K. K.; Schmidt, J. J. *Nano Lett.* **2008**, *8*, 3029–3034.

(57) Mathé, J.; Aksimentiev, A.; Nelson, D. R.; Schulten, K.; Meller, A. *Proc. Natl. Acad. Sci. U. S. A.* **2005**, *102*, 12377–12382.

(58) Butler, T. Z.; Gundlach, J. H.; Troll, M. *Biophys. J.* **2007**, *93*, 3229–3240.

(59) Muzard, J.; Martinho, M.; Mathé, J.; Bockelmann, U.; Viasnoff, V. *Biophys. J.* **2010**, *98*, 2170–2178.

(60) Zhang, X.; Price, N. E.; Fang, X.; Yang, Z.; Gu, L. Q.; Gates, K. S. *ACS Nano* **2015**, *9*, 11812–11819.

(61) Wang, J.; Yi, X.; Tang, H.; Han, H.; Wu, M.; Zhou, F. *Anal. Chem.* **2012**, *84*, 6400–6406.

(62) Mitchell, P. S.; Parkin, R. K.; Kroh, E. M.; Fritz, B. R.; Wyman, S. K.; Pogosova-Agadjanyan, E. L.; Peterson, A.; Noteboom, J.; O'Briant, K. C.; Allen, A.; Lin, D. W.; Urban, N.; Drescher, C. W.; Knudsen, B. S.; Stirewalt, D. L.; Gentleman, R.; Vessella, R. L.; Nelson, P. S.; Martin, D. B.; Tewari, M. *Proc. Natl. Acad. Sci. U. S. A.* **2008**, *105*, 10513–10518.

(63) McAlexander, M. A.; Phillips, M. J.; Witwer, K. W. *Front. Genet.* **2013**, *4*, 83.

(64) Nguyen, M. A.; Srijanto, B.; Collier, C. P.; Retterer, S. T.; Sarles, S. A. *Lab Chip* **2016**, *16*, 3576–3588.

(65) Czekalska, M. A.; Kaminski, T. S.; Jakiela, S.; Tanuj Sapra, K.; Bayley, H.; Garstecki, P. *Lab Chip* **2015**, *15*, 541–548.

(66) Friddin, M. S.; Smithers, N. P.; Beaugrand, M.; Marcotte, I.; Williamson, P. T.; Morgan, H.; de Planque, M. R. *Analyst* **2013**, *138*, 7294–7298.

(67) Zagnoni, M. *Lab Chip* **2012**, *12*, 1026–1039.

(68) Steinbock, L. J.; Radenovic, A. *Nanotechnology* **2015**, *26*, 074003.

(69) Feng, Y.; Zhang, Y.; Ying, C.; Wang, D.; Du, C. *Genomics, Proteomics Bioinf.* **2015**, *13*, 4–16.

Figure 1

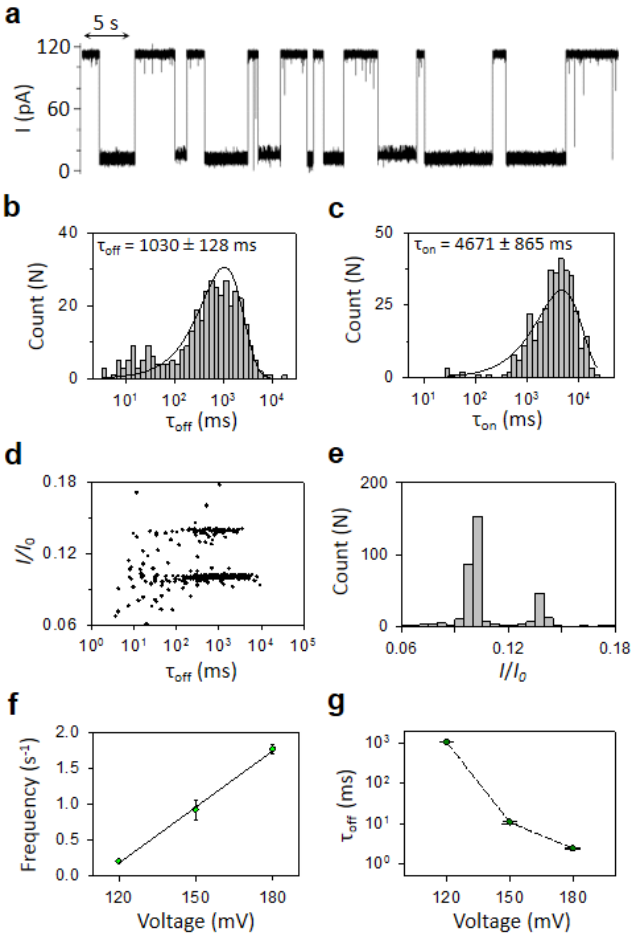

Figure 1. Nanopore resistive pulse sensing of 100 nM miD155–P155 duplex in symmetrical 1 M KCl at +120 mV. (a) Representative αHL current trace, showing an open-pore current (I_0) of ~115 pA interrupted by resistive pulses down to ~10–15 pA (~0.1 I/I_0). The duration of these pulses reflects the time required for the duplex to unzip. (b,c) The wide range of interevent durations and event dwell times reflects the stochastic nature of duplex-nanopore interactions. Histogram fitting with an exponential logarithmic probability function gives an interevent interval τ_{on} of 4671 ± 865 ms and a dwell time τ_{off} of 1030 ± 128 ms. (d) Individual resistive pulses vary significantly in level-1 dwell time but cluster around two distinct residual current amplitudes (I/I_0). (e) The histogram of the residual nanopore current shows that the deeper current block events occur more frequently than the shallower current block events (Table S4).

(f) The event frequency increases linearly with the applied potential between +120 mV and +180 mV. (g) The level-1 event dwell time reduces dramatically when the applied potential is increased to +180 mV.

Figure 2

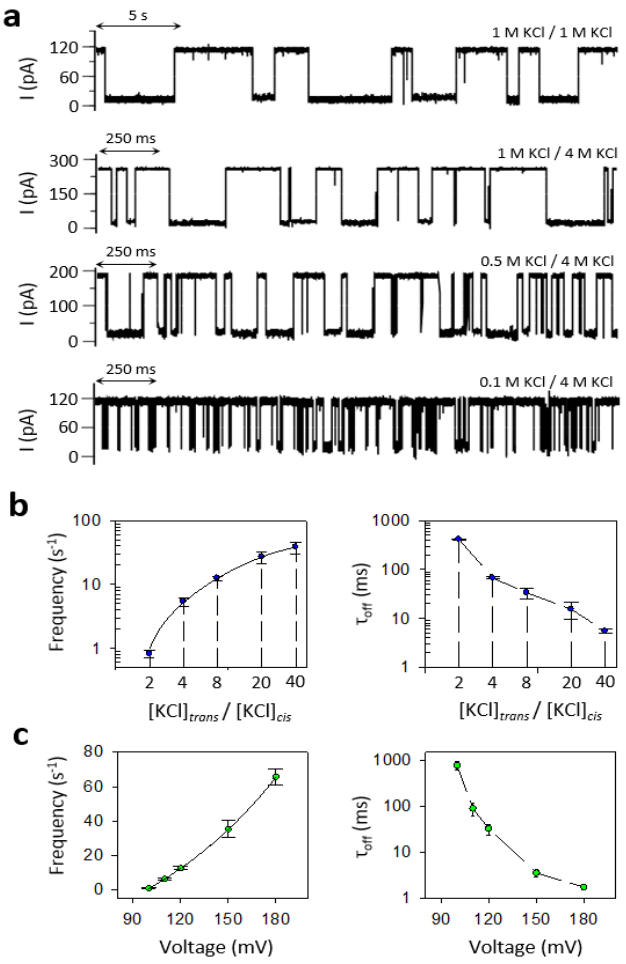

Figure 2. Characterization of KCl gradients for 100 nM miD155–P155 duplex. (a) Representative αHL current traces for symmetrical 1 M KCl and for 1 / 4 M, 0.5 / 4 M and 0.1 / 4 M *cis*/*trans* KCl gradients, recorded at +120 mV. Large gradients result in significantly shorter duplex level-1 dwell times and significantly higher duplex capture rates. (b) Capture rates and dwell times for five different KCl gradients at +120 mV. (c) Capture rates and level-1 dwell times for the 0.5 / 4 M KCl gradient as a function of the applied potential. Standard deviations are derived from independent experiments.

Figure 3

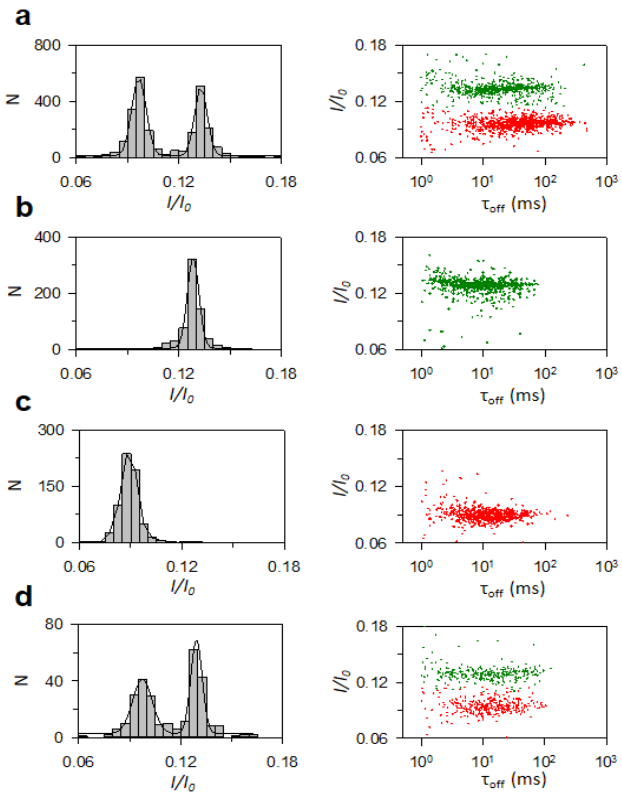

Figure 3. Level-1 current block levels and dwell times for miD155 hybridized to single-overhang probes. (a) The P155 double-overhang probe gives a bimodal distribution of nanopore-duplex interaction events. The deeper current block events (0.097 I/I_0) events had a mean duration of 56.4 ms and the dwell time of the shallower block events (0.133 I/I_0) was 31.3 ms. (b) Duplexes with the P155-5'-$(dC)_{30}$ probe resulted in a single current block level of 0.128 I/I_0 with a mean dwell time of 12.6 ms. (c) Duplexes with $(dC)_{30}$-3'-P155 gave a single current block level of 0.096 I/I_0 with a 13.4 ms dwell time. (d) A mixture of 50 nM miD155 – P155-5'-$(dC)_{30}$ duplex and 50 nM miD155 – $(dC)_{30}$-3'-P155 duplex mimicked the event distribution observed for 100 nM duplex with the double-overhang $(dC)_{30}$-P155-$(dC)_{30}$ probe. All experiments were performed with a 0.5 / 4 M KCl gradient and at +120 mV. Unless otherwise noted all duplexes are present at 100 nM concentration.

Figure 4

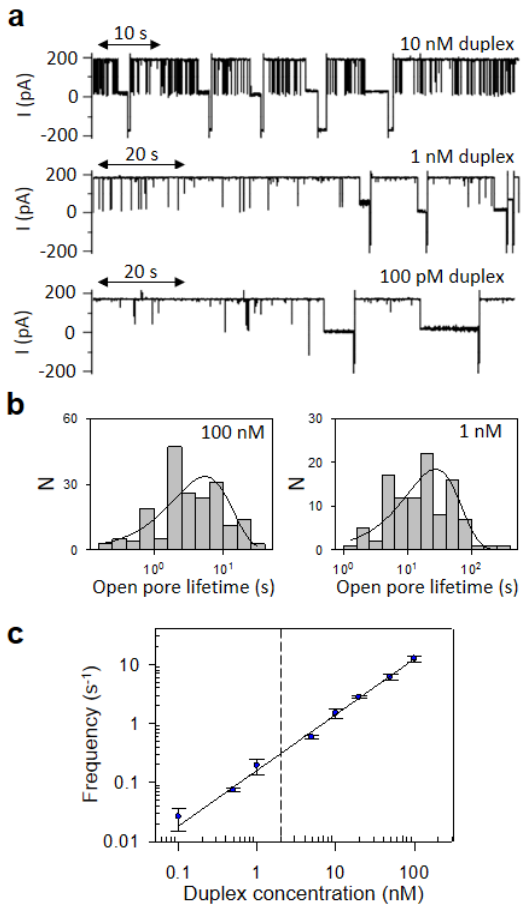

Figure 4. Capture rate at lower duplex concentrations for 0.5 / 4 M *cis*/*trans* KCl at +120 mV. (a) Representative current traces for 10 nM, 1 nM and 100 pM miD155–P155 duplex. Negative currents indicate brief periods where the potential was switched to -120 mV to re-open the pore. Most pore closures with 10 nM duplex were caused by pore clogging (~0.1 I/I_0) whereas the pore closures with 1 nM and 100 pM duplex (no residual current) occurred spontaneously. (b) Histograms of the duration of open-pore episodes, obtained in multiple experiments, for 100 nM and 1 nM duplex. The mean open-pore duration as determined from log probability distribution fits is 5.4 ± 2.6 s and 27 ± 9.5 s in the presence of 100 nM and 1 nM duplex, respectively. (c) Log-log plot of nanopore capture frequency versus duplex concentration. Event frequencies for 10–100 nM duplex were determined by histogram fitting and frequencies for 0.1–1 nM duplex

were determined by dividing the number of events over the open-pore recording time. Standard deviations are derived from independent experiments. Linearity is observed for four orders of magnitude in duplex concentration, as indicated by a power-law fit (solid line, $R^2 = 0.9988$).

Table 1. Resistive pulse parameters for miD155–P155 with different symmetrical and asymmetrical *cis*/*trans* electrolyte solutions[a]

$[XCl]_{cis}$	$[XCl]_{trans}$	τ_{off} (ms)	τ_{on} (ms)	frequency (s^{-1})
1 M KCl	1 M KCl	1030 ± 128	4671 ± 865	0.21 ± 0.04
1 M NaCl	1 M NaCl	1211 ± 131	3735 ± 518	0.27± 0.04
1 M CsCl	1 M CsCl	907 ± 114	3385 ± 834	0.30 ± 0.07
1 M NH_4Cl	1 M NH_4Cl	1120 ± 173	2026 ± 333	0.49 ± 0.08
1 M LiCl	1 M LiCl	> 20,000	–	–
0.5 M KCl	4 M KCl	33.3 ± 2.2	82 ± 14.6	12.2 ± 2.2
0.5 M CsCl	4 M CsCl	44.5 ± 5.8	85 ± 17.7	11.8 ± 2.4
0.5 M LiCl	4 M LiCl	> 5,000	–	–
0.5 M LiCl	4 M KCl	71.4 ± 14.4	102 ± 12.5	9.8 ± 1.2

[a] Dwell time, interevent interval and event frequency for 100 nM miD155–P155 duplex at +120 mV.

Table 2. Resistive pulse parameters for miD155 hybridized to P155 probes with different $(dC)_{30}$ modifications[a]

DNA probe	I/I_0 (level 1)	events	τ_{off} (ms)	τ_{on} (ms)	f_{on} (s^{-1})
$(dC)_{30}$-5'-P155	0.128 ± 0.4%	all	12.6 ± 2.4	106.9 ± 17	9.57 ± 1.8
P155-3'-$(dC)_{30}$	0.096 ± 4%	all	13.4 ± 1.9	97.2 ± 18	10.56 ± 1.9
$(dC)_{30}$-P155-$(dC)_{30}$	0.096 ± 8%	55%	42.4 ± 11.2	–	–
	0.131 ± 7%	45%	22.9 ± 8.4	–	–
		all	33.5 ± 9.0	80.52 ± 6.98	12.49 ± 1.02

[a] For 100 nM duplex in 0.5 / 4 M *cis*/*trans* KCl at +120 mV.